Admittance-adaptive model-based approach to mitigate biodynamic feedthrough

Venrooij, Joost; Mulder, Max; Mulder, Mark; Abbink, David A.; van Paassen, Marinus M.; van der Helm, Frans C T; Bulthoff, Heinrich H.

DOI
10.1109/TCYB.2016.2601638

Publication date
2017

Document Version
Final published version

Published in
IEEE Transactions on Cybernetics

Admittance-Adaptive Model-Based Approach to Mitigate Biodynamic Feedthrough

Joost Venrooij, *Member, IEEE*, Max Mulder, Mark Mulder, *Member, IEEE*, David A. Abbink, *Senior Member, IEEE*, Marinus M. van Paassen, *Senior Member, IEEE*, Frans C. T. van der Helm, and Heinrich H. Bülthoff, *Member, IEEE*

***Abstract*—Biodynamic feedthrough (BDFT) refers to the feedthrough of vehicle accelerations through the human body, leading to involuntary control device inputs. BDFT impairs control performance in a large range of vehicles under various circumstances. Research shows that BDFT strongly depends on adaptations in the neuromuscular admittance dynamics of the human body. This paper proposes a model-based approach of BDFT mitigation that accounts for these neuromuscular adaptations. The method was tested, as proof-of-concept, in an experiment where participants inside a motion simulator controlled a simulated vehicle through a virtual tunnel. Through evaluating tracking performance and control effort with and without motion disturbance active and with and without cancellation active, the effectiveness of the cancellation was evaluated. Results show that the cancellation approach is successful: the detrimental effects of BDFT were largely removed.**

***Index Terms*—Biodynamic feedthrough (BDFT), mitigation, neuromuscular adaptation, neuromuscular admittance.**

I. Introduction

BIODYNAMIC feedthrough (BDFT) refers to the phenomenon where vehicle accelerations feed through the human body and cause involuntary limb motions which, in turn, result in involuntary control inputs [1], [2]. BDFT is a problem for a large range of vehicles and occurs under very different conditions [3]–[8]. It reduces comfort, control performance and in some cases even safety is impaired. Finding ways to mitigate or cancel this phenomenon is important.

BDFT has been studied for several decades. Already in the earlier studies it was recognized that BDFT is a complex problem of which the details are only poorly understood [9]. This conclusion is in many ways still true today. Throughout the years various sources of influence have been identified and although steady progress was made in understanding them, there are still many unanswered questions.

A main motivator for research is the desire to *reduce* the BDFT effects on manual control performance. Several mitigation techniques have been suggested. For instance, an active vibration isolation system was developed [10], [11], which isolates the human operator (HO) from vehicle accelerations by actively compensating for platform accelerations. A similar approach is used in recent work on backhoe excavators [8]. An adaptive filtering technique was proposed in [12] and tested in [13]. Results of another approach, force reflection, which cancels BDFT effects by opposing the involuntary forces it causes, are presented in [14]. This technique was also successfully used in [15]. In [16], a robust controller to suppress BDFT effects using μ-synthesis was developed. These examples illustrate the fact that a range of studies have been devoted to BDFT mitigation and that many different ways of achieving that goal exist. For a review of the possible BDFT mitigation methods, the reader is referred to [17].

This paper aims to contribute to the existing body of knowledge regarding BDFT mitigation, by proposing and experimentally evaluating a novel mitigation approach: an admittance-adaptive, model-based signal cancellation technique. The most important contribution of this technique is the inclusion of an important influence on BDFT dynamics that has thus far not, or at least not systematically, been accounted for in other mitigation schemes: the adaptive neuromuscular dynamics of the human body.

Human body dynamics vary between persons, for example due to different body sizes and weights, and also within one person over time. Humans can adapt their body's neuromuscular dynamics through muscle co-contraction and modulation of reflexive activity in response to, e.g., task instruction, workload, and fatigue [18]. The highly variable human body dynamics are amongst the most influential, complex and poorly understood causes for BDFT variability [19], [20]. For a successful mitigation of BDFT, these variabilities must be understood and accounted for [21].

The mitigation approach proposed here is *model-based*: it relies on a model to "predict" the involuntary BDFT-induced control inputs. Mitigation is done using *signal cancellation*, that is, by subtracting the predicted involuntary input from

Manuscript received May 27, 2015; revised October 23, 2015 and June 10, 2016; accepted August 10, 2016. Date of publication September 12, 2016; date of current version November 15, 2017. The work of D. Abbink was supported by NWO through VENI under Grant 10650, in part by Nissan, in part by Boeing, in part by "H-Haptics" Research Program, and in part by VIDI. This paper was recommended by Associate Editor S. Hu.

J. Venrooij and H. H. Bülthoff are with the Department of Human Perception, Cognition and Action, Max Planck Institute for Biological Cybernetics, 72076 Tübingen, Germany (e-mail: joost.venrooij@tuebingen.mpg.de).

M. Mulder and M. M. van Paassen are with the Faculty of Aerospace Engineering, Delft University of Technology, 2629 HS Delft, The Netherlands.

M. Mulder, D. A. Abbink, and F. C. T. van der Helm are with the Faculty of Mechanical, Maritime and Materials Engineering, Delft University of Technology, 2628 CD Delft, The Netherlands.

Color versions of one or more of the figures in this paper are available online at http://ieeexplore.ieee.org.

Digital Object Identifier 10.1109/TCYB.2016.2601638

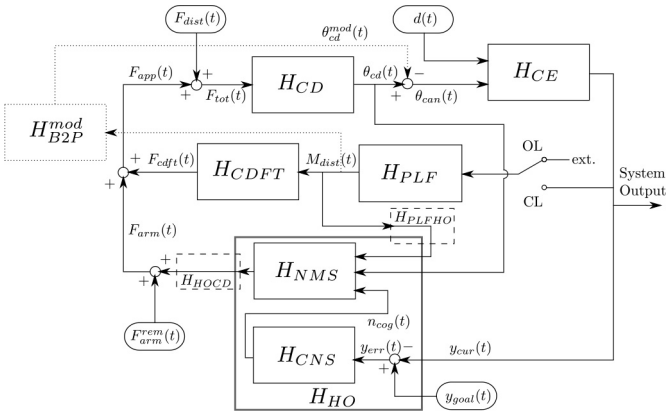

Fig. 1. BDFT system model. An HO controls a CE using a CD. Motion disturbances $M_{\text{dist}}(t)$ are coming from the PLF. The feedthrough of $M_{\text{dist}}(t)$ to involuntary applied forces $F_{\text{arm}}(t)$ and involuntary CD deflections $\theta_{\text{cd}}(t)$ is called BDFT. The feedthrough of $M_{\text{dist}}(t)$ to inertia forces $F_{\text{cdft}}(t)$ is called CDFT. $F_{\text{app}}(t)$ is the sum of the forces applied to the CD by the HO. The HO consists of a CNS and an NMS. The connection between the HO and the environment is governed by two "interfaces," H_{PLFHO} and H_{HOCD}. The CE and PLF can form an OL or CL system. In this paper, a BDFT model $H_{\text{B2P}}^{\text{mod}}$ is used to estimate the involuntary part of the CD deflections, $\theta_{\text{cd}}^{\text{mod}}(t)$. This signal is subtracted from the total CD deflections $\theta_{\text{cd}}(t)$ to cancel BDFT.

the total input—which contains both voluntary and involuntary components—BDFT is canceled. This in contrast to the alternative technique of force cancellation, where the involuntary force is reflected by the control device (CD). Finally, the approach is *admittance-adaptive*, a term used here to indicate the model's ability to account for changes in the settings of the neuromuscular system (NMS). The NMS dynamics are commonly described through the neuromuscular admittance [22].

The novel admittance-adaptive feature of the proposed BDFT mitigation approach will be implemented in an elementary fashion, as a proof-of-concept. We used an experimental setup where participants inside a motion simulator were asked to fly a simulated vehicle through a virtual tunnel, a so-called "highway-in-the-sky" (HITS). Through measurements with and without motion disturbances active, and with and without cancellation active, the method was evaluated.

This paper is structured as follows. Section II introduces the BDFT system model that stands at the basis of our research. Some general considerations regarding BDFT mitigation are provided in Section III. Based on these, our mitigation approach is discussed in Section IV, followed by an experimental description, Section V. Results are discussed in Section VI; this paper ends with the conclusions in Section VII.

II. Biodynamic Feedthrough System Model

The BDFT system model [23], shown in Fig. 1, includes all high-level elements that play a role in the BDFT phenomenon. This general *system* model is different from the *specific* BDFT model, which will be introduced shortly and aims to describe a particular part of the BDFT phenomenon for cancellation purposes. Fig. 1 indicates this latter part as $H_{\text{B2P}}^{\text{mod}}$.

Each model block in Fig. 1 contains a transfer function (indicated with H) describing the dynamics of the system it represents. The HO is controlling a controlled element (CE) by comparing the current state $y_{\text{cur}}(t)$ with a certain goal state $y_{\text{goal}}(t)$. The CE can be perturbed by a disturbance signal, $d(t)$, for which the operator should correct. The operator can control the state of the CE by means of a CD. Commands are applied by exerting forces, $F_{\text{arm}}(t)$, on the CD, resulting in a deflection, $\theta_{\text{cd}}(t)$, which enters the CE.

Motion disturbances $M_{\text{dist}}(t)$ typically originate from the motion of a vehicle, referred to as the platform (PLF). These disturbances affect the human-machine system in two ways: 1) CD feedthrough (CDFT), where the CD mass converts the PLF accelerations to inertia forces $F_{\text{cdft}}(t)$ and 2) BDFT, where the PLF accelerations induce unintentional limb motions, causing involuntary forces applied to the CD, which in turn result in involuntary CD deflections. Note that BDFT includes the occurrence of both involuntary forces and involuntary deflections (positions). To distinguish between these two related effects, it is proposed in [1] to refer to them as BDFT to forces (B2F) and BDFT to positions (B2P), respectively.

In model-based BDFT cancellation, one can cancel either involuntary forces or involuntary positions, which requires a B2F or B2P dynamics model, respectively. The solution proposed here involves signal cancellation (in contrast to force cancellation), and hence requires a B2P dynamics model.

A BDFT system can be classified as being "closed-loop" (CL) or "open-loop" (OL), depending on whether the operator's inputs influence the PLF motion, or not. Both CL and OL BDFT systems are important, and are included in Fig. 1 by a switch. In case of an OL BDFT system, the input to the PLF can be regarded as external (denoted as "ext." in Fig. 1). This paper only considers OL systems; the BDFT system model can be adapted to also represent CL systems.

The HO block can be split into the central nervous system (CNS), and NMS [18]. The CNS consists of the brain and spinal cord of the HO and is responsible for all cognitive control commands, mainly involving *voluntary* control inputs; CNS commands are neurally transmitted to the NMS through $n_{\text{cog}}(t)$. The NMS represents the dynamics of the limb, connected to the CD, and contains body parts such as bones, muscles, etc. The interface H_{PLFHO} describes the dynamics of the connection between the PLF and the HO, involving, for example, seat suspension or the effect of seat belts. These dynamics are sometimes referred to as the "seat transmissibility" and determine how accelerations enter the operator's body. The interface H_{HOCD} describes the dynamics of the connection between HO and CD, e.g., grip visco-elasticity or the effects of an arm rest. This interface determines how limb motions result in applied forces $F_{\text{arm}}(t)$.

The neuromuscular admittance, providing an estimate of the neuromuscular limb dynamics, can be measured using a force disturbance $F_{\text{dist}}(t)$, also shown in Fig. 1. Neuromuscular admittance represents limb dynamics by describing the relation between a force input and a position output of a limb [22]. Note that admittance is not part of the BDFT problem itself, but obtaining it can be relevant because BDFT dynamics depend on neuromuscular admittance [1], [20].

With two disturbance inputs $M_{\text{dist}}(t)$ and $F_{\text{dist}}(t)$ active, the CD deflection signal $\theta_{\text{cd}}(t)$ has a number of components

$$\theta_{\text{cd}}(t) = \theta_{\text{cd}}^{F\text{dist}}(t) + \theta_{\text{cd}}^{M\text{dist}}(t) + \theta_{\text{cd}}^{\text{cog}}(t) + \theta_{\text{cd}}^{\text{rem}}(t) \qquad (1)$$

where superscripts $^{F\text{dist}}$ and $^{M\text{dist}}$ mark the contributions of the force and motion disturbances. Note that $\theta_{\text{cd}}^{M\text{dist}}(t)$ is the involuntary part of the control input caused by the acceleration signal, i.e., the BDFT effect. The superscript $^{\text{cog}}$ denotes the cognitive part in the CD deflection, i.e., the deflection due to voluntary control actions coming from H_{CNS}. The remaining part, the remnant, is denoted with the superscript $^{\text{rem}}$. It can be defined as the operator's control output that is not linearly correlated with the system inputs (here the disturbance signals) [24]. In our BDFT system model, remnant originates from the remnant force signal $F_{\text{arm}}^{\text{rem}}(t)$.

Model-based signal cancellation is indicated in Fig. 1 with dotted lines: motion disturbance signal $M_{\text{dist}}(t)$ forms the input for the BDFT model $H_{\text{B2P}}^{\text{mod}}$. The model output, $\theta_{\text{cd}}^{\text{mod}}(t)$, represents an *estimate* of the involuntary part of CD deflections $\theta_{\text{cd}}^{M\text{dist}}(t)$, and is subtracted from the total CD deflection signal $\theta_{\text{cd}}(t)$. The result is a "corrected" CD deflection signal, $\theta_{\text{can}}(t)$, which enters the CE. If the contribution $\theta_{\text{cd}}^{M\text{dist}}(t)$ is largely canceled by $\theta_{\text{cd}}^{\text{mod}}(t)$, the cancellation is successful. Note that through signal cancellation, the actual, physical deflection of the CD is *not* changed, only the input to the CE is adjusted. Also note that if cancellation is *not* active, $\theta_{\text{can}}(t)$ is equal to $\theta_{\text{cd}}(t)$.

III. Mitigation Considerations

A. Between- and Within-Subject Variability

BDFT is known to depend on many different factors [9]. Using Fig. 1 they can be broadly identified. Some examples: the CD dynamics H_{CD} affect how involuntary forces result in involuntary deflections [9], [25]; adding or removing an armrest changes the H_{HOCD} dynamics and with that the BDFT dynamics [26], [27]. There are many more factors which play a role, but when considering BDFT for one particular vehicle, with a certain cockpit layout, most of these influencing factors become invariant.

An important exception to this is the HO. The variabilities between and within HOs renders BDFT a variable, dynamic relationship, both varying *between* different persons (between-subject variability), but also *within* one person over time (within-subject variability). Previous research suggests that for a successful model-based cancellation of BDFT, both between- and within-subject variability need to be taken into account, as otherwise the cancellation might fail [21].

What This Implies: For successful cancellation, the BDFT model needs to be both *personalized* for each participant and *adapted* to the situation at hand.

B. Types of Biodynamic Feedthrough

Before constructing a BDFT model, a choice needs to be made regarding which type of BDFT dynamics is to be modeled. Venrooij *et al.* [25] proposed that the BDFT response can be separated in several related dynamical relationships, such as B2P and B2F [1].

The former, B2P, describes the transfer dynamics from vehicle accelerations (e.g., in m/s^2) to involuntary CD deflections (e.g., in rad). For the latter, B2F, two variations exist. One way of obtaining B2F is determining the dynamics between vehicle accelerations M_{dist} (in m/s^2) and forces $F_{\text{arm}}(t)$ (in N). These dynamics are labeled B2F in CL (B2FCL) as the force signal $F_{\text{arm}}(t)$ is contained in a CL system. Another way of obtaining B2F is by "opening" this loop and calculating the transfer dynamics between accelerations and the OL force applied to the CD (not shown in Fig. 1). This OL force is that part of the force signal $F_{\text{arm}}(t)$ which is directly and solely due to the acceleration disturbances; these dynamics are called B2F in OL (B2FOL) (see [1], [2] for details).

For signal cancellation—the type of cancellation applied here—a B2P model is required. As was argued in [23], there are several benefits in exploiting the relationship between B2P and B2FCL$^+$ dynamics in this case. It can be shown that[1]

$$H_{\text{B2P}}(s) = H_{\text{CD}}(s)H_{\text{B2FCL}}^{+}(s) \qquad (2)$$

implying that the B2P dynamics can be easily obtained from the B2FCL$^+$ dynamics. So, by constructing the model on B2FCL$^+$ data and then multiplying the model with the known and fixed CD dynamics, a B2P model is obtained [1], [23]. It should be noted that the same approach and experiment can be used to validate a force cancellation approach, using a B2FOL$^+$ model. This is not pursued in this paper.

What This Implies: For signal cancellation, a B2P model is required, which can be obtained through a B2FCL$^+$ model, multiplied with the known CD dynamics.

C. Neuromuscular Admittance

Neuromuscular admittance represents limb dynamics by describing the relation between a force input and a position output of a limb. The admittance can vary strongly through muscle co-contraction and modulation of reflexive activity in response to, e.g., task instruction, workload, and fatigue [18]. As humans in actual vehicle control tasks also change their neuromuscular settings to the task at hand, these variations in BDFT dynamics need to be accounted for.

What This Implies: Successful model-based BDFT cancellation requires the model to account for variability in the BDFT dynamics due to neuromuscular adaptations; this feature can be referred to as an *admittance-adaptive* capability.

D. Role of Cognitive Corrective Inputs

Little is known about how *voluntary* cognitive control inputs affect the involuntary BDFT-induced control inputs. One generally assumes that an HO is capable of correcting for at least parts of involuntary inputs. As human control capabilities are limited in bandwidth, it is safe to assume that these cognitive corrections are also limited up to a certain frequency, e.g., to 1 Hz [28]. To determine how exactly an HO realizes cognitive BDFT corrections, e.g., whether these are based on

[1]Note that this relationship makes use of so-called "uncorrected" B2FCL dynamics, indicated with a superscripted $^+$. The dynamics are not corrected for CDFT dynamics. As the final goal is to create a B2P model, correcting the B2FCL dynamics is not required (see [1]).

visual or proprioceptive information, or how they depend on workload and task difficulty, requires more research.

The effects of cognitive corrective inputs are not the focus of this paper, but nevertheless, their presence may have some implications for the cancellation approach proposed here. Especially for the measurements in which data are obtained to construct the BDFT cancellation models, the *identification measurements*, the presence of cognitive corrective inputs can be, in fact, detrimental. If the operator invests cognitive control effort in correcting (a part of) the BDFT effects, these effects are thus removed from the BDFT measurements. As a consequence, any BDFT model based on these data will not model these and, when using this model in model-based BDFT cancellation, will not correct for them either. This means that the *same* amount of cognitive control effort will be required from the operator whether mitigation is active or not, as these effects will still have to be corrected manually. In other words, the harder the participant works in the identification measurements, the "lazier" the BDFT model will become.

What This Implies: The presence of cognitive corrective inputs requires special attention, especially in the identification measurements on which the BDFT models are based.

IV. Mitigation Approach

A. Highway-in-the-Sky

This paper is loosely based on a rotorcraft application, without burdening the experiment with the complexities of realistic helicopter flight simulation. The CDs were those used in typical helicopters; the simulated vehicle dynamics were highly simplified helicopter roll dynamics. Participants were asked to fly this vehicle through an HITS, i.e., a virtual tunnel [29].

The HITS representation was chosen for two reasons. First, it provides a close-to-realistic vehicle control task, where a vehicle moves through 3-D space. The tunnel image provides performance bounds and reference to current and future target positions [29], similar to many real-life vehicle control tasks.

Second, the HITS provides a means to *impose an adaptation* of the neuromuscular dynamics on the participant. By changing the size of the tunnel frames, the performance bounds can be altered [29]: in a narrow tunnel, pilots will need to increase co-contraction and reflexive activity to stay inside the tunnel, and vice versa. This change occurs largely intuitively, but by additionally instructing participants to react to the changes in the tunnel frames, a robust way of changing NMS dynamics during the experiment was obtained.

B. Neuromuscular Adaptation

In our experiment, the HITS consisted of square tunnel frames of two sizes and colors: 1) wide white frames and 2) narrow red frames. The instruction for both types of frames was to stay inside the tunnel. For the wide white tunnel this should be done with minimum control effort, largely ignoring the exact vehicle position within the tunnel and only steering when necessary to remain inside the tunnel. For the narrow red tunnel, the instruction was to follow the center of the tunnel frames as closely as possible, requiring maximum control effort.

With these task instructions, the "optimal" NMS settings varied between "passive relaxed" and "active stiff." These settings correspond to two of the classic NMS tasks [30]: 1) the "relax task" (RT), with the instruction to use a passive neuromuscular setting of the arm while holding the CD and 2) the "position task" (PT), with the instruction to use a stiff setting of the NMS to keep the position of the CD in the centered position. Hence, an HITS section with wide white tunnel frames is referred to as an "RT section," one with narrow red frames as an "PT section."

C. Model Development Step 1: Identification Measurements

In the first step, the *identification measurements*, BDFT dynamics were measured for each participant while performing classic relax and PTs, a method used in many previous studies (see [20]). These measurements formed the basis of two BDFT models: one representing BDFT dynamics in the RT sections, the other the BDFT dynamics in the PT sections. In a later stage these models served to "predict" the involuntary control inputs (see Fig. 1). To minimize the role of cognitive corrective inputs, no visual feedback was provided. Participants were still able to perform the instructed control tasks, as they only relate to how the neuromuscular setting of the arm responds to force disturbances [30].

D. Model Development Step 2: Parameter Estimation

In the second step, the data of the identification measurements were used to develop two B2P models. The model structure and parameter estimation approach are described in detail in [23]. In short, the approach uses a modeling technique referred to as "asymptote modeling": by combining a number of base functions, with particular asymptotic characteristics, the measured B2FCL$^+$ dynamics can be accurately modeled in the frequency domain. This method yields a mathematical model with 16 parameters, and the following model structure:

$$H^{\text{mod}}_{\text{B2FCL}}(s) = KH^1_B(s)H^2_B(s)H^3_B(s)H^4_B(s)H^5_B(s) \tag{3}$$

where s is the Laplace operator, K is a scaling gain, and the H^k_B terms are the base functions (where k is the base function number). Each base function has the following structure:

$$H^k_B(s, f_{nk}, \zeta_k, \gamma_k) = \left(1 + 2\zeta_k/(2\pi f_{nk})s + s^2/(2\pi f_{nk})^2\right)^{\gamma_k} \tag{4}$$

where f_{nk} is the natural frequency [Hz], ζ_k the damping factor [−], and γ_k the order [−]. Note that if $\gamma_k = -1$ the base function describes typical mass-spring-damper dynamics. Venrooij *et al.* [23] showed that the orders of the five base functions can be chosen as

$$\gamma_1 = -1,\ \gamma_2 = +2,\ \gamma_3 = -2,\ \gamma_4 = +2 \text{ and } \gamma_5 = -1.$$

The remaining parameters of each base function are obtained by fitting the model on the measured B2FCL$^+$ dynamics (using MATLAB's `lsqnonlin` function). Multiplying the obtained model with the known CD dynamics yields the B2P model [compare with (2)]

$$H^{\text{mod}}_{\text{B2P}}(s) = H_{\text{CD}}(s)H^{\text{mod}}_{\text{B2FCL}}(s). \tag{5}$$

As the CD dynamics are described with three parameters, the resulting B2P model contains 19 parameters.

E. Model Development Step 3: Implementation

In this paper, the adaptation of the model to the two neuromuscular settings, PT and RT, was implemented using a simple switching strategy based on the vehicle location in the HITS. When positioned in a PT section, the PT model was used (was "active"); in an RT section, the RT model was used.

This switching strategy is still far from a truly adaptive approach, where the model parameters would be adapted in real-time, based on a continuous measurement of the neuromuscular dynamics. Currently, the techniques required to accurately and robustly obtain these measurements are under development [31], [32]. Hence, as a proof-of-concept, the approach is implemented in this elementary fashion. Proving that successful cancellation is possible using this suboptimal approach will provide additional confidence that the concept itself is sound and can be improved as new techniques emerge.

Finally, it should be noted that in this experiment, the participant only controlled the virtual vehicle and *not* the motion of the simulator. Hence, the acceleration disturbance M_{dist} was not affected by the operator's control inputs, an "OL" situation which allowed us to accurately measure the BDFT dynamics also during the cancellation experiment.

F. Cancellation Experiment: Conditions

The cancellation experiment had two independent variables: 1) the task (TSK) and 2) condition (COND). The two TSK levels were PT and RT. There were four COND levels: the condition in which the cancellation was active will be referred to as the cancellation condition (CAN). In addition, two baseline conditions were used: 1) a static condition (STA), in which no acceleration disturbances were applied (simulator not moving) and 2) a motion condition (MOT), in which acceleration disturbances were applied but cancellation was inactive. Comparing control performance between the STA, MOT, and CAN conditions provides insight in how the acceleration disturbances cause the performance to deteriorate and how much of the original performance can be restored with cancellation.

To investigate the importance of within-subject variability and the effects of neuromuscular settings on cancellation, a fourth condition was added, in which the cancellation was done in an "incongruent" fashion, i.e., the PT model was applied in the RT HITS sections and viceversa. This condition will be referred to as the incongruent condition (INC).

V. Experimental Description

A. Hypotheses

The experiment aimed at testing three hypotheses.

1) *The BDFT Hypothesis:* BDFT will occur in the MOT and will result in decreased control performance and increased effort as compared to the STA.
2) *The Cancellation Hypothesis:* With cancellation active (CAN), performance will improve, effort will decrease as compared to the condition without cancellation (MOT); performance and effort are partially restored to the values obtained in the STA.
3) *The Incongruency Hypothesis:* Incongruent cancellation (INC) leads to lower performance and higher effort than obtained with congruent cancellation (CAN).

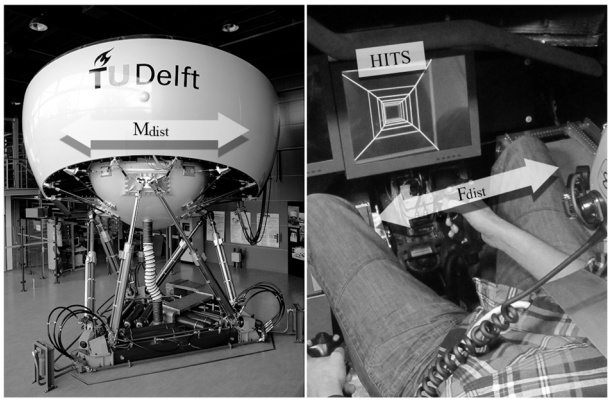

Fig. 2. Experimental setup used in this paper. A participant (right) seated inside the SRS (left) uses a helicopter cyclic to control a virtual vehicle. The screen shows an HITS. A motion disturbance, $M_{\text{dist}}(t)$, perturbs the motion-base of the simulator in lateral direction. A force disturbance, $F_{\text{dist}}(t)$, perturbs the cyclic in lateral direction.

TABLE I
Data of Participants ($N = 11$)

	Age [years]	Weight [kg]	Height [cm]	BMI [kg/m^2]
Mean	26.0	77.9	183.6	23.1
SD	3.9	11.9	8.6	2.9
Range	21-35	57-100	172-196	19.3-27.8

B. Apparatus

The experiment was performed in TU Delft's SIMONA Research Simulator (SRS) [33]. The CDs were electrically-actuated helicopter controls (collective and cyclic) with adjustable dynamics. For this experiment only the cyclic roll axis was used for lateral control inputs. The cyclic roll stick had a length 650 [mm], stiffness 1.000 [N/deg], damping 0.0516 [Ns/deg], and inertia 0.0162 [Ns^2/deg]; no nonlinearities were simulated.

A helicopter seat was used, in which the participants were strapped-in with a five-point safety belt. Visual information was displayed on a head-down display (15-in LCD, 1024×768 pixels, 60 Hz refresh rate) in front of the participant. Fig. 2 shows the experimental setup.

C. Participants

Data were collected for 11 male participants (Table I). One participant was left-handed, all others were right-handed. Their body mass index (BMI) was calculated by dividing a person's weight (in kg) by height squared (in m^2), and is a measure of the total amount of body fat in adults [34]. Values between 19 and 25 are considered to be normal (mesomorph) [34]. Two participants had higher values (endomorph).

TABLE II
REPETITIONS PER CONDITION

Straight HITS				
	STA	MOT	CAN	INC
PT	3	3	3	×
RT	3	3	3	×
Curved HITS				
	STA	MOT	CAN	INC
PT	6	6	6	6
RT	6	6	6	6

D. Experimental Execution

Participants received task instructions before entering the simulator. Once installed in the simulator, the participants received training (approx. 10 min). To familiarize the participant with the vehicle dynamics, the HITS and the tasks, the first training run was performed without motion in a straight HITS with several RT and PT sections. The second training was performed in the same HITS, but with the motion disturbance activated. In the third and fourth training run, the participant was presented with a curved HITS. In these runs, participants were instructed to attain a consistent and repeatable neuromuscular setting in the different sections.

After training, the participant's BDFT dynamics were measured in the identification measurements. Here, no visual information was displayed, and participants performed, in random order, five RTs and five PTs. When these were completed, the participant received a break of approximately 10 min, during which the model parameters were estimated.

In the cancellation experiment, participants were presented with both straight and curved HITS sections (more details will follow). Table II shows the number of repetitions per condition for each participant. A 10 min break was held after completing one-third and two-thirds of the total number of repetitions.

E. Vehicle Dynamics

The vehicle that the participants controlled moved forward at a constant speed of 25 m/s (≈50 knots); its dynamics represented highly-simplified helicopter roll dynamics. These simplified dynamics were used for two main reasons. First, they resulted in a direct coupling between control inputs and vehicle response, yielding a strong correspondence between inputs and performance, making performance a more reliable metric. Second, because of the simple vehicle dynamics, the experiment could be performed by nonexpert pilots, which facilitated data collection.

The vehicle responded only to lateral control inputs (roll). As can be seen in Fig. 1, the input for the vehicle dynamics was the signal $\theta_{\text{can}}(t)$, which was either equal to the CD deflection $\theta_{\text{cd}}(t)$ (in the STA and MOT conditions), or the difference between $\theta_{\text{cd}}(t)$ and the output of the BDFT model, $\theta_{\text{cd}}^{\text{mod}}(t)$ (in the CAN and INC conditions). The vehicle roll angle ϕ was directly coupled to the control input

$$\phi(t) = K_\phi \theta_{\text{can}}(t) \tag{6}$$

where K_ϕ is the roll gain, set to 0.05.

TABLE III
CURVED HITS PARAMETERS: CUR-XXYY REFERS TO A CURVED HITS, CONSISTING OF AN XX SECTION, FOLLOWED BY A YY SECTION

	K_s [m]	f_1 [m^{-1}]	f_2 [m^{-1}]	p_1 [deg]	p_2 [deg]
CUR-PTRT	100	$8 \cdot 10^{-4}$	$4 \cdot 10^{-4}$	180	12
CUR-RTPT	100	$8 \cdot 10^{-4}$	$4 \cdot 10^{-4}$	-20	0

Every time step, the vehicle heading $\psi(t)$ was updated through numeric integration of the roll angle

$$\psi(t) = \psi(t - \Delta t) + K_\psi \phi(t) \Delta t \tag{7}$$

where K_ψ is the heading gain and Δt is the simulation time step (0.01 s). In this paper, the heading gain was set at 5.0.

F. HITS Configuration

The HITS tunnel frames were 25 m apart, such that at a speed of 25 m/s approximately one frame would pass every second. The width and height of the RT section frames were 25 m, for the PT sections this was 5 m.

Four different HITS were used during the experiment.

1) *STR-PT:* A straight HITS consisting of a PT section.
2) *STR-RT:* A straight HITS consisting of an RT section.
3) *CUR-PTRT:* A curved HITS with a PT section, followed by an RT section.
4) *CUR-RTPT:* A curved HITS with an RT section, followed by a PT section.

Each RT and PT section consisted of 50 frames. In addition, each tunnel started with a straight lead-in section of five frames. The CUR tunnels had an additional straight lead-out section of five frames. In total, the STR tunnels had a length of 55 frames (5+50), the CUR tunnels had a length of 110 frames ($5+50+50+5$). During the cancellation experiment, the different HITS were presented in random order. Each HITS was repeated three times for each participant and each condition, yielding the number of repetitions listed in Table II. Note that the CUR-type HITS contained both a PT and RT section, so three repetitions of both CUR-types resulted in six repetitions of the PT and RT condition.

The HITS trajectory was defined in an x-z coordinate frame. The curved trajectory was constructed by summing two sinusoids with a chosen frequency and phase shift

$$x = K_s \sum_{k=1}^{2} \sin\left(2\pi f_k z + p_k \frac{\pi}{180}\right) \tag{8}$$

where K_s is a scaling gain, z are values of the z-coordinate, and f_k and p_k are the frequency and phase shift of the sinusoid, respectively. The chosen parameters are listed in Table III. The frequencies f_1 and f_2 were chosen low enough to not require any high frequency control inputs. With a speed of 25 m/s, the required steering frequency to follow the individual sinusoids were 0.02 and 0.01 Hz, respectively, well below the frequency content of the two disturbance signals (discussed below). The difference between CUR-PTRT and CUR-RTPT, apart from the order of the PT and RT sections, was a phase shift. In the analysis, the results obtained in the CUR-PTRT and CUR-RTPT tunnels are combined.

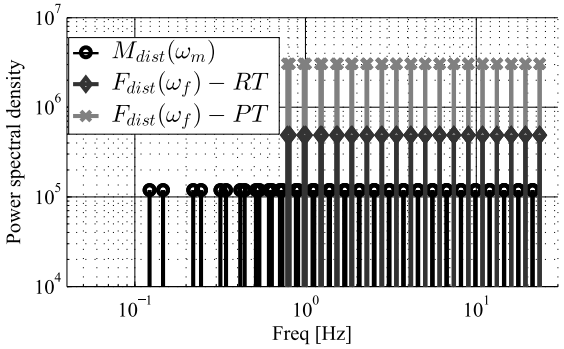

Fig. 3. PSD of the two disturbance signals M_{dist} and F_{dist}. The magnitude of F_{dist} was varied between the RT and PT sections.

G. Disturbance Signals

In the cancellation experiment, two disturbance signals were applied simultaneously: 1) a motion disturbance signal $M_{\text{dist}}(t)$ on the simulator's motion base and 2) a force disturbance signal $F_{\text{dist}}(t)$ on the CD (Fig. 2). The former signal was used to determine the BDFT (B2P and B2FCL$^+$) dynamics, the latter signal was used to determine the NMS admittance.

Both disturbance signals were multisines, defined by their frequency components. The length of the disturbance signals for the STR tunnels (with 55 frames) was 60 s, and for the longer CUR tunnels (110 frames) 120 s. These signal lengths were sufficient for the experiment.

The disturbance signals were separated in frequency, to allow distinguishing the response due to each disturbance in the measured signals [20], [30]. The frequency content of the disturbance signals was equal in all conditions. For the motion disturbance signal $M_{\text{dist}}(t)$, 24 logarithmically-spaced pairs of frequency points, referred to as ω_m, were chosen between 0.1 and 21.4 Hz. The force disturbance $F_{\text{dist}}(t)$ was applied to measure admittance, a secondary objective. Hence, to minimize the influence of $F_{\text{dist}}(t)$ on control behavior and performance, the frequency range of $F_{\text{dist}}(t)$ was limited to high frequencies only: 18 logarithmically-spaced pairs of frequency points were chosen between 0.78 and 23.5 Hz; these frequency points are referred to as ω_f. There existed no overlap between ω_m and ω_f. Fig. 3 shows the power-spectral-densities (PSDs) of the two disturbance signals.

The gain used for the $M_{\text{dist}}(t)$ signal was 0.8, resulting in a maximum acceleration of 3.67 m/s^2, maximum velocity of 1.12 m/s and a maximum position 0.72 m. For the force disturbance F_{dist}, the gain for the PT section was 5.0, and for the RT section 2.0 (note the difference in magnitude in Fig. 3). The gain was varied for two main reasons: 1) to keep the standard deviations of the CD deflections in the RT and PT sections approximately similar [20] and 2) as a "haptic reminder" of the change in task, that is, the increase in force gain helped participants to attain a stiffer neuromuscular setting in the PT sections. Gains were tuned to obtain high squared coherences for the admittance estimates [20].

H. Calculating B2P and B2FCL

The applied force $F_{\text{app}}(t)$ and the CD deflection $\theta_{\text{cd}}(t)$ were measured, together with the vehicle state, i.e., its position, heading angle, roll angle, etc. In the analysis, signals $F_{\text{dist}}(t)$ and $M_{\text{dist}}(t)$ were used as commanded (not directly measured), and were cut to a length of 2^{12} samples (=40.96 s). This allowed calculating the frequency response functions of the B2P and B2FCL dynamics (see [20]).

B2P dynamics were estimated using the estimated cross-spectral density between $M_{\text{dist}}(t)$ and $\theta_{\text{cd}}(t)$ ($\hat{S}_{m\text{dist},\theta}(j\omega_m)$) and the estimated auto-spectral density of $M_{\text{dist}}(t)$ ($\hat{S}_{m\text{dist},m\text{dist}}(j\omega_m)$)

$$\hat{H}_{\text{B2P}}(j\omega_m) = \frac{\hat{S}_{m\text{dist},\theta}(j\omega_m)}{\hat{S}_{m\text{dist},m\text{dist}}(j\omega_m)} \tag{9}$$

where $\hat{H}_{\text{B2P}}(j\omega_m)$ is the estimate on frequencies ω_m of the B2P dynamics $H_{\text{B2P}}(s)$, with s the Laplace variable.

B2FCL$^+$ dynamics were calculated using the estimated cross-spectral density between $M_{\text{dist}}(t)$ and $F_{\text{app}}(t)$ and the estimated auto-spectral density of $M_{\text{dist}}(t)$

$$\hat{H}^{+}_{\text{B2FCL}}(j\omega_m) = \frac{\hat{S}_{m\text{dist},f}(j\omega_m)}{\hat{S}_{m\text{dist},m\text{dist}}(j\omega_m)} \tag{10}$$

where $\hat{H}^{+}_{\text{B2FCL}}(j\omega_m)$ is the estimate of the actual B2FCL$^+$ dynamics $H^{+}_{\text{B2FCL}}(s)$ on frequencies ω_m. Note that by using the $F_{\text{app}}(t)$ signal, and not $F_{\text{arm}}(t)$, the $\hat{H}^{+}_{\text{B2FCL}}(j\omega_m)$ dynamics are not corrected for CDFT dynamics. As the dynamics are meant to be used to construct a B2P model [using (5)] such a correction is not required.

Neuromuscular admittance was estimated using $F_{\text{dist}}(t)$, but as these estimates will not be the subject of discussion here, the interested reader is referred to [20].

I. Performance Metrics

Two model performance metrics and two task performance metrics were defined to quantify: 1) the model error; 2) the cancellation quality; 3) the HITS tracking performance; and 4) the control effort.

1) Model Error Metric: To quantify the model error, the sum of the squared logarithmic error was calculated between the measured and modeled B2P dynamics [35]

$$E = \sum \left| \log\left(\frac{\hat{H}_{\text{B2P}}(j\omega_m)}{H^{\text{mod}}_{\text{B2P}}(j\omega_m)} \right) \right|^2. \tag{11}$$

2) Cancellation Metric: A cancellation percentage, introduced in [21], was computed which indicates how much of the involuntary control inputs were canceled. This is evaluated by quantifying how much of the BDFT effects were removed when the model output $\theta^{\text{mod}}_{\text{B2P}}(t)$ was subtracted from the total CD deflection $\theta_{\text{cd}}(t)$. Using a frequency-decomposition technique [20], the total CD deflection $\theta_{\text{cd}}(t)$ can be decomposed in three parts

$$\theta_{\text{cd}}(t) = \theta^{F\text{dist}}_{\text{cd}}(t) + \theta^{M\text{dist}}_{\text{cd}}(t) + \theta^{\text{res}}_{\text{cd}}(t) \tag{12}$$

that is, a contribution of F_{dist}, a contribution of M_{dist}, and a residual, *res*. The residual is the sum of the cognitive and remnant contributions [see (1)]. The components of (12) were calculated by evaluating the PSD of $\theta_{\text{cd}}(t)$, on either ω_f, on ω_m or on all remaining frequencies. Through taking the

inverse fast Fourier transform of these PSDs, the time series were obtained (see [20] for details). Applying the same operation, the components of $\theta_{\text{can}}(t)$—the signal obtained after subtracting $\theta_{\text{B2P}}^{\text{mod}}(t)$—could be obtained.

The cancellation percentage P_{can} was introduced in [21] as the ratio of the root-mean-square (RMS) of $\theta_{\text{can}}^{M\text{dist}}$ and $\theta_{\text{cd}}^{M\text{dist}}$, which represent the M_{dist} component before and after the cancellation was applied

$$P_{\text{can}} = \left(1 - \frac{\text{RMS}\left(\theta_{\text{can}}^{M\text{dist}}(t)\right)}{\text{RMS}\left(\theta_{\text{cd}}^{M\text{dist}}(t)\right)}\right) \cdot 100\%. \tag{13}$$

With a good B2P model, $\theta_{\text{can}}^{M\text{dist}}(t)$ will be small compared to the original $\theta_{\text{cd}}^{M\text{dist}}(t)$ and P_{can} will be close to 100%. In cases where the model is not as accurate, cancellation is less and P_{can} will be lower or even negative.

3) Error Metric: Tracking performance was expressed using the average absolute heading error, μ_{ψ_e}. Heading error equals the difference between the current vehicle heading ψ and the target heading ψ_{tar}, defined as the heading of the section between the two frames where the vehicle is located

$$\mu_{\psi_e} = \frac{1}{N}\sum_{k=1}^{N}|\psi_{\text{tar}}(k) - \psi(k)| \tag{14}$$

where N is the number of measurement samples. Note that a high value implies a low tracking performance.

The heading error shows how well participants were able to follow the tunnel, independently from the actual position within the tunnel. In other words, participants were not penalized for being left or right from the center (or, in fact, inside or outside the tunnel) but rather for not aligning the vehicle heading with the tunnel heading.

The reason for using heading error rather than position error, is that the latter is not representative for task performance in this experiment. In the RT sections, the instruction was to stay inside the HITS using minimal control effort, allowing a participant to use the full width of the tunnel; here, a position error would be inadequate to evaluate task performance.

4) Control Effort Metric: As a measure for control effort, the RMS of the derivative of the CD deflections (the steering speed) was calculated. To improve the reliability of this measure as a metric for effort, the residual CD deflections $\theta_{\text{cd}}^{\text{res}}(t)$ were used [see (12)]. By using the residual component, instead of the complete CD deflection signal, the direct effects (i.e., the feedthrough) of the two disturbance signals were removed. This improves the reliability of the metric as direct feedthrough is not related to control effort. $\theta_{\text{cd}}^{\text{res}}(t)$ consists of the sum of the cognitive control inputs and remnant. Control effort was defined as

$$E_{\dot{\theta}_{\text{res}}} = \text{RMS}\left(\dot{\theta}_{\text{cd}}^{\text{res}}(t)\right) \tag{15}$$

where $\dot{\theta}_{\text{cd}}^{\text{res}}(t)$ is the time derivative of $\theta_{\text{cd}}^{\text{res}}(t)$.

VI. Results and Discussion

In the following, first the results for the curved HITS (CUR) will be presented in detail. Results for the straight HITS (STR) are then briefly discussed; these have been reported in [36].

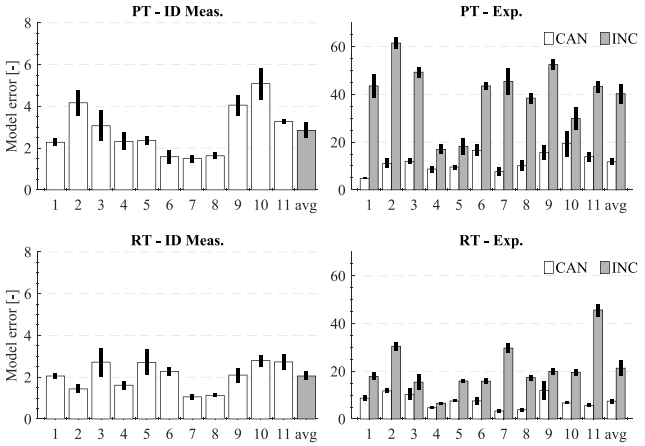

Fig. 4. Average model error for each participant (11 participants) and across participants (avg) for the identification measurements (left column) and during the cancellation experiment (right column). The bars indicated the mean and the lines indicate the standard error of the mean.

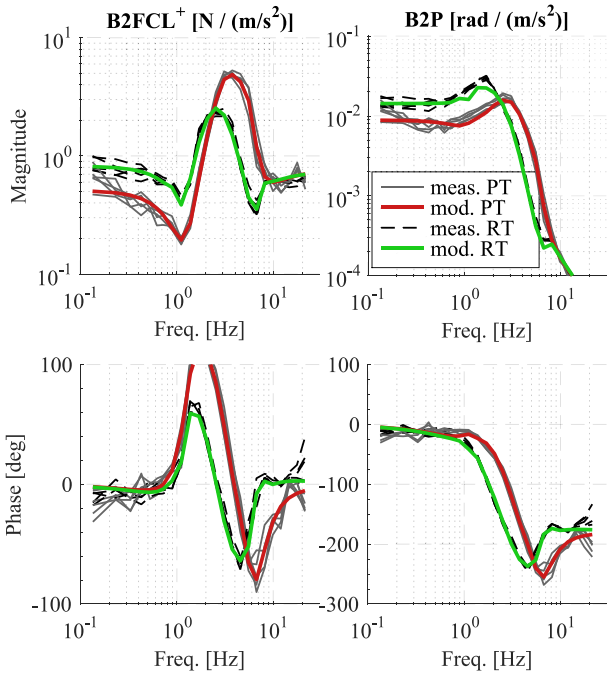

Fig. 5. Measured and modeled B2FCL^{+} and B2P dynamics for participant #7, obtained in the identification measurements. This participant showed small variations between trials and large differences between the PT and RT conditions.

A. Model Error Metric

Fig. 4 shows the average model error E (11) for the identification measurements (left column) and for the cancellation experiment (right column). The bars indicate the mean, the lines indicate the standard error of the mean. The results obtained for the identification measurements (left column) show that the model error for the PT varies between 1.50 and 5.10 and has an average (μ) of 2.85 and a standard deviation (σ) of 1.19. The RT varies between 1.05 and 2.79 and has a lower average ($\mu = 2.10$) and standard deviation ($\sigma = 0.66$).

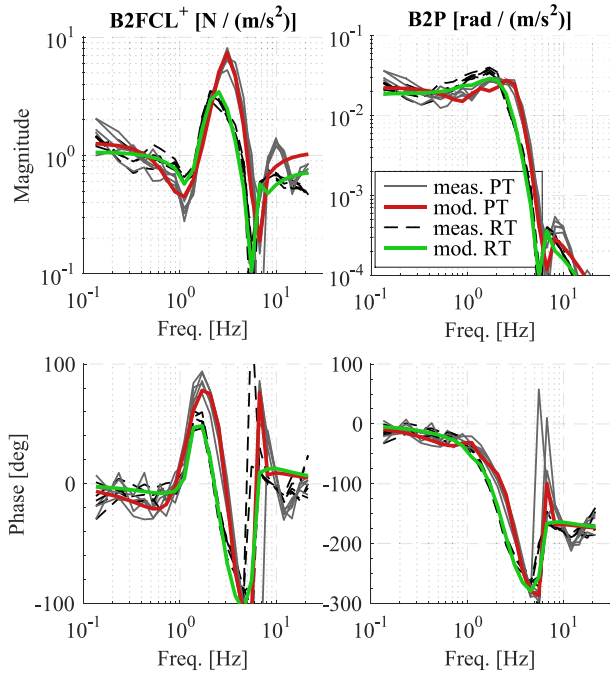

Fig. 6. Measured and modeled B2FCL$^+$ and B2P dynamics for participant #10, obtained in the identification measurements. This participant showed larger variations between trials and smaller differences between the PT and RT conditions than participant #7.

A deeper insight in the quality of the model can be obtained by looking at the measured and modeled dynamics for the participants with the lowest and highest model error, i.e., participants #7 and #10, respectively. Fig. 5 shows the measured B2FCL$^+$ and B2P dynamics obtained during the identification measurements for participant #7. The five repetitions for each task resulted in very similar B2FCL$^+$ and B2P dynamics, which indicates consistency in the execution of the tasks. Clear differences in dynamics *between* the two tasks can be observed, illustrating the within-subject variability in BDFT dynamics. The dynamics of the PT and RT models, obtained by performing a parameter fit on the time average of the five repetitions, are also shown in Fig. 5. The models describe the measured dynamics well, resulting in a low model error.

Fig. 6 shows result for participant #10, who had the largest model error. There are slightly larger variations between trials, but the model fits are still accurate. From this, it can be concluded that the B2FCL$^+$ and B2P dynamics were accurately captured, even for the participant with the largest model error. It should be noted that the differences between the RT and PT dynamics are much smaller for participant #10. In other words, this participant did not vary his/her neuromuscular behavior as much as participant #7. This illustrates that an accurate description of the BDFT dynamics indeed requires *personalized* model parameters.

The right column of Fig. 4 shows the model error during the cancellation experiment for both CAN and INC conditions. Note the difference in scale on the y-axes between the two columns. For the CAN condition, the model error quantifies the difference between the modeled B2P dynamics for a task and the B2P dynamics that were actually measured during

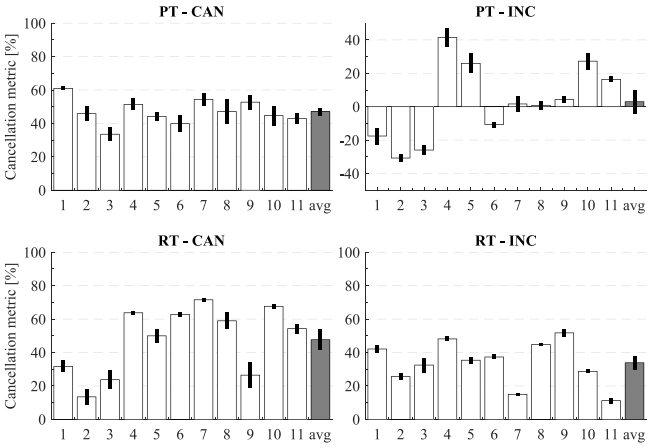

Fig. 7. Percentage of BDFT cancellation for each participant (11 participants) and the average (avg), for the PT and RT sections (row) and the CAN and INC conditions (column), curved HITS. The bars indicated the mean and the lines indicate the standard error of the mean.

that task. A small error indicates an accurate model. For the INC condition, the error quantifies the difference between the modeled B2P dynamics for one task and the B2P dynamics that were actually measured during the other task. A large error indicates a large difference between the B2P dynamics of the two tasks. It can be observed that for each participant the model error increases from PT-CAN to PT-INC. This is reflected in the average values: for PT-CAN the average $\mu = 11.76$ ($\sigma = 4.29$), while for PT-INC $\mu = 40.24$ ($\sigma = 13.71$). The results are similar for RT: for each participant the model error for RT-INC is always larger than the model error for RT-CAN. The average for RT-CAN $\mu = 7.47$ ($\sigma = 2.99$) and for RT-INC $\mu = 21.29$ ($\sigma = 10.44$). In summary, these results show that the model error is always larger for incongruent models than for congruent models, which is fully in line with expectations.

B. Cancellation Metric

Results for the cancellation metric are given in Fig. 7, which shows the average (bars) and standard error of the mean (lines) of P_{can} (13), obtained for the six repetitions of the PT and RT sections in the CAN and INC conditions for each participant. For both PT and RT case, congruent cancellation (CAN) yielded a positive cancellation percentage in all conditions. For PT-CAN, the level of cancellation achieved varies between 33.5% and 61.0%, with $\mu = 47.0\%$ and $\sigma = 7.5\%$. For RT-CAN, the average is similar ($\mu = 47.6\%$) but the spread is much larger and cancellation varies between 13.4% and 71.6% ($\sigma = 20.2\%$). It can be concluded that for the PT a fairly robust result was obtained; cancellation was successful for each participant. For the RT, results vary much more between participants.

In the INC condition, for both PT and RT tasks the cancellation reduces compared to the CAN condition. Analysis of variance (repeated measures) showed a significant reduction in cancellation percentage from CAN to INC ($F(1, 10) = 59.4$, $p < 0.001$) and from PT to RT ($F(1, 10) = 29.3$, $p < 0.001$). Furthermore, a significant interaction between

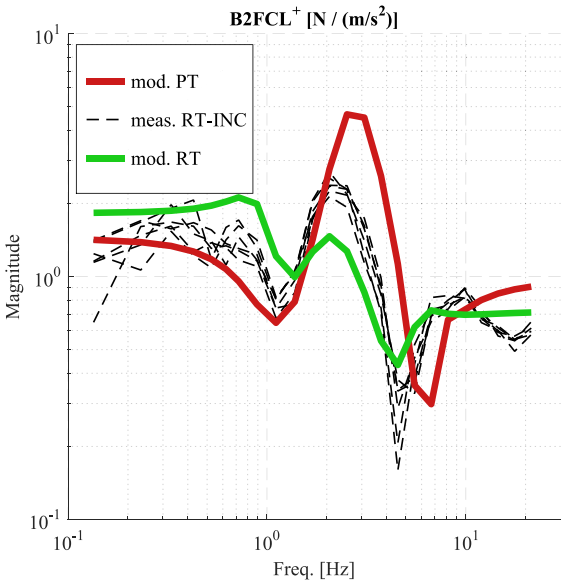

Fig. 8. Measured and modeled B2FCL$^+$ dynamics in the INC condition for participant #1. This participant shows a mismatch between modeled and actual RT dynamics due to different behavior between the identification measurements and the cancellation experiment.

condition and task was found ($F(1, 10) = 5.51$, $p < 0.05$), caused by the fact that the INC condition shows a much larger effect on the PT task than on the RT task. For PT-INC ($\mu = 3.0\%$, $\sigma = 23.2\%$) and the cancellation percentage for some participants became negative, meaning that incongruent cancellation decreased instead of improved performance.

Overall, the RT-INC condition has lower cancellation levels ($\mu = 33.9\%$, $\sigma = 13.0\%$) than the RT-CAN condition. However, for four participants the cancellation is higher: participants #1–#3 and #9 (note that these are also the participants with the lowest RT-CAN results). From Fig. 4, it can be seen that the RT models for these participants were not of poorer quality than for other participants (recall that participant #10 showed the largest model error). Instead, these results can be explained by the fact that these participants behaved differently in the identification measurements and the cancellation experiment. In other words, in the RT-INC condition, these participants attained a "stiffer" NMS setting than during the identification measurements, making the PT model more appropriate.

Fig. 8 shows the measured B2FCL$^+$ dynamics (magnitude only), obtained for the RT-INC condition, and the participant's model dynamics for participant #1. Note that the PT model, which was applied in the INC condition, matches fairly well with the measured dynamics at low frequencies (<2 Hz). Hence, even though an RT was instructed, this participant behaved stiffer, i.e., closer to the PT, such that the PT model used in the RT-INC condition yielded better cancellation than the RT model in the RT-CAN condition. Several participants showed the tendency of performing a stiffer RT in the cancellation experiment than in identification measurements, in both RT-CAN and RT-INC conditions, but this effect was strongest for participants #1–#3 and #9.

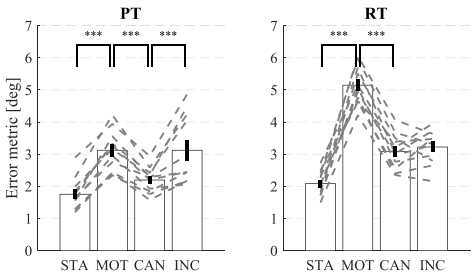

Fig. 9. Tracking performance for the four conditions (PT and RT sections), curved HITS. The bars indicated the mean and the lines indicate the standard error of the mean. The dashed gray lines connect the mean values obtained for each participant. "***" indicates $p < 0.001$.

The above leads us to conclude that, overall, the cancellation was successful. Four participants expressed different RT behavior between the identification measurements and the cancellation experiment, which led to the unexpected result that cancellation results in the RT-INC condition were better than in the RT-CAN condition. This issue was already touched upon earlier as a possible weakness of the current approach, in which the BDFT dynamics are not monitored online during the cancellation experiment. However, this should not be considered as a discouraging result. In fact, the observation that the participants that show fairly poor cancellation results in the RT-CAN condition show better results in the RT-INC condition further strengthens the conclusion that a model that better matches with the *actual* BDFT dynamics provides better cancellation results.

C. Tracking Error Metric

Fig. 9 shows the error metric (averaged absolute heading error, where high values mean low performance) for all conditions: STA, MOT, CAN, and INC. In this figure and the following, dashed gray lines connect the mean values obtained for each participant; bars show the mean across all participants, with the black lines the standard error of the mean. Analysis of variance (repeated measures) showed a significant difference between conditions ($F(3, 30) = 141.5$, $p < 0.001$) and tasks ($F(1, 10) = 25.2$, $p < 0.001$) and a significant interaction between conditions and tasks ($F(3, 30) = 26.9$, $p < 0.001$).

Comparing the results for the STA and MOT conditions, for each participant the heading error increased with motion present. That is, BDFT effects deteriorated tracking performance considerably. A contrast on this difference was calculated for both PT and RT conditions and was significant [PT: $t(30) = 8.01$, $p < 0.001$ and RT: $t(30) = 20.30$, $p < 0.001$].

Results obtained for the CAN condition indicate that, for all participants, performance *improved* due to the cancellation. For many participants the error metric approximates the value obtained in the STA condition, signifying considerable benefit from the cancellation. Contrasts between the MOT and CAN conditions were significant, for both PT and RT sections [PT: $t(30) = 5.42$, $p < 0.001$ and RT: $t(30) = 13.71$, $p < 0.001$]. This confirms that the cancellation was indeed successful.

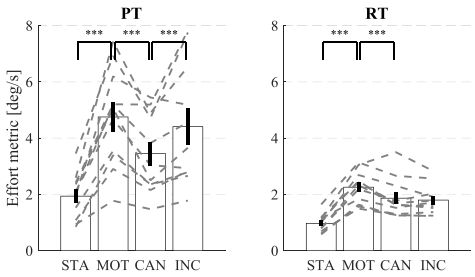

Fig. 10. Control effort for the four conditions (PT and RT sections), curved HITS. The bars indicated the mean and the lines indicate the standard error of the mean. The dashed gray lines connect the mean values obtained for each participant. *** indicates $p < 0.001$.

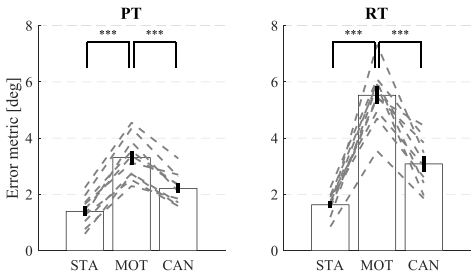

Fig. 11. Tracking performance for the three conditions (PT and RT sections), straight HITS. The bars indicated the mean and the lines indicate the standard error of the mean. The dashed gray lines connect the mean values obtained for each participant. *** indicates $p < 0.001$.

The importance of having an admittance-adaptive approach, which matches the cancellation to the current NMS dynamics of the operator, is signified by the fact that for the PT the INC condition yielded an increase in the error metric, i.e., a deteriorated performance, compared to the CAN condition. Here, the contrast between the CAN and INC conditions was significant ($t(30) = 5.42$, $p < 0.001$). For the RT, the differences between CAN and INC are smaller, and in some cases the INC even shows a slightly better performance (participants #1, #2, and #9). These are the same participants which showed better cancellation levels for the RT-INC than the RT-CAN condition, Fig. 7. For the RT, the contrast between the CAN and INC conditions was not significant ($t(30) = 0.951$, $p = 0.174$).

In conclusion, the performance data confirm the three experimental hypotheses. Performance deteriorates due to BDFT but can be largely restored when cancellation is active. In the PT, participants performed better with congruent cancellation than with incongruent cancellation.

D. Effort Metric

Fig. 10 shows the effort metric (average RMS of the CD deflection derivative) for the four conditions: 1) STA; 2) MOT; 3) CAN; and 4) INC. Here a high value indicates a high effort. Analysis of variance (repeated measures) showed a significant difference between conditions ($F(3, 30) = 35.7$ $p < 0.001$) and tasks ($F(1, 10) = 34.6$, $p < 0.001$) and a significant interaction between conditions and tasks ($F(3, 30) = 13.44$, $p < 0.001$). Effort increased, for all participants, from the STA to the MOT condition. The contrast on this difference is significant for both PT and RT case [PT: $t(30) = 8.10$, $p < 0.001$ and RT: $t(30) = 11.32$, $p < 0.001$]. It can be concluded that the addition of motion significantly increased control effort. Note the difference in the values of the effort metric obtained for the PT and RT; the much lower values in the RT task is in agreement with the task instruction to use "minimum effort."

Cancellation in the CAN condition significantly decreased control effort [PT: $t(30) = 3.75$, $p < 0.001$ and RT: $t(30) = 3.44$, $p < 0.001$], for some participants back to the no-motion level (STA). In the CAN condition, only one participant (#2) showed higher effort with respect to the MOT condition, for all other participants effort decreased. Comparing the CAN and INC conditions, results for the PT showed a significant increase in effort ($t(30) = 2.76$, $p < 0.001$); in the RT, however, no significant difference was found ($t(30) = 0.59$, $p = 0.278$).

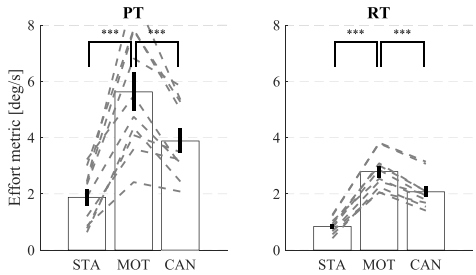

Fig. 12. Control effort for the three conditions (PT and RT sections), straight HITS. The bars indicated the mean and the lines indicate the standard error of the mean. The dashed gray lines connect the mean values obtained for each participant. *** indicates $p < 0.001$.

Although the control effort metrics show a larger spread than observed for the performance metric, overall the hypotheses are confirmed. Effort increases due to BDFT effects but can be significantly reduced when cancellation is active. For the PT, control effort was lower with congruent cancellation than with incongruent cancellation.

E. Straight HITS Sections

In the straight HITS conditions, cancellation yielded a positive percentage for all conditions and all participants. For PT-CAN, the cancellation level varied between 36.7% and 60.4% [average (μ) 49.3% and standard deviation (σ) of 9.0%]. For RT-CAN the average is similar ($\mu = 50.9\%$) but the variability between participants is considerably larger; P_{can} varies between 15.0% and 73.8% ($\sigma = 21.1\%$). The same participants as in the CUR conditions (#1–#3 and #9) showed the lowest cancellation results in the RT-CAN condition.

Figs. 11 and 12 show the tracking performance and control effort metrics, respectively. The trends in these metrics were the same at those found for the curved HITS conditions, with similar levels of statistical significance. For a detailed discussion, the reader is referred to [36].

The results obtained from the STR tunnels lead to the same conclusions regarding the BDFT hypothesis and the cancellation hypothesis as were obtained for the CUR tunnels. The successful cancellation of BDFT in both straight and curved

tunnels, using the same BDFT model, demonstrates the robustness of the approach and provides further evidence of its applicability.

VII. Conclusion

Regarding the hypotheses tested in the experiment, the following conclusions can be drawn.

1) *The BDFT Hypothesis Was Confirmed:* BDFT occurred in the MOT and significantly deteriorated tracking performance and increased control effort with respect to the STA.
2) *The Cancellation Hypothesis Was Confirmed:* With cancellation (CAN) the tracking error and control effort were significantly lower than without the cancellation (MOT).
3) *The Incongruency Hypothesis Was Only Partially Confirmed:* Incongruent cancellation (INC) leads to lower performance and higher effort than obtained with congruent cancellation (CAN) for the PT only.

The current results may raise the question what the added value is of having an admittance-adaptive approach at all, as the PT model seems to perform fine in both conditions. In fact, in an earlier publication [21], it was already predicted that "the "safest" model choice appears to be the PT model, as it shows a partial reduction, even across tasks" (p. 1675). In the same publication it is added, however, that the level of cancellation that can be achieved with a PT model is lower than that which can be achieved with a task-specific model.

In the analysis it was shown that some participants executed the RT task differently in the identification measurements and the cancellation experiment. This led to a poor match between the BDFT model and the actual BDFT dynamics for these participants and this explains why the RT-INC showed better results than the RT-CAN condition for some participants. This illustrates the importance of using a BDFT model that matches the *actual* BDFT dynamics, i.e., the actual task that is performed.

In this paper only two types of control tasks were studied, the PT and RT. Evidently, an HO is capable of many different types of control behavior, each with its influence on the setting of the neuromuscular dynamics and thus on the BDFT dynamics. Studying the success of cancellation across a wider range of these possible settings is likely to show the benefit, if not the necessity, of an adaptive cancellation approach that matches the neuromuscular setting as closely as possible. This issue can only be properly addressed with *online* identification techniques that allow for real-time adaptation of the cancellation model to the current settings of the NMS. These methods are currently under development [31], [32]. Issues regarding the implementation and certification of such BDFT cancellation systems, e.g., aerospace vehicles, are to be addressed in future research.

References

[1] J. Venrooij *et al.*, "A framework for biodynamic feedthrough analysis—Part I: Theoretical foundations," *IEEE Trans. Cybern.*, vol. 44, no. 9, pp. 1686–1698, Sep. 2014.

[2] J. Venrooij *et al.*, "A framework for biodynamic feedthrough analysis—Part II: Validation and application," *IEEE Trans. Cybern.*, vol. 44, no. 9, pp. 1699–1710, Sep. 2014.

[3] R. Gabel and G. J. Wilson, "Test approaches to external sling load instabilities," *J. Amer. Helicopter Soc.*, vol. 13, no. 3, pp. 44–54, 1968.

[4] D. Banerjee, L. M. Jordan, and M. J. Rosen, "Modeling the effects of inertial reactions on occupants of moving power wheelchairs," in *Proc. Rehab. Eng. Assistive Tech. Soc. North America Conf. (RESNA)*, Salt Lake City, UT, USA, Jun. 1996, pp. 220–222.

[5] R. A. Hess, "Theory for roll-ratchet phenomenon in high-performance aircraft," *J. Guid. Control Dyn.*, vol. 21, no. 1, pp. 101–108, 1998.

[6] D. L. Raney, E. B. Jackson, C. S. Buttrill, and W. M. Adams, "The impact of structural vibration on flying qualities of a supersonic transport," in *Proc. AIAA Atmospheric Flight Mech. Conf.*, Montreal, QC, Canada, Aug. 2001, pp. 1–11.

[7] R. B. Walden, "A retrospective survey of pilot-structural coupling instabilities in naval rotorcraft," in *Proc. Amer. Helicopter Soc. 63rd Annu. Forum*, Virginia Beach, VA, USA, May 2007, pp. 897–914.

[8] H. C. Humphreys, W. J. Book, and K. M. Feigh, "Development of controller-based compensation for biodynamic feedthrough in a backhoe," *Proc. Inst. Mech. Eng. I J. Syst. Control Eng.*, vol. 228, no. 2, pp. 107–120, 2014.

[9] R. W. McLeod and M. J. Griffin, "Review of the effects of translational whole-body vibration on continuous manual control performance," *J. Sound Vib.*, vol. 133, no. 1, pp. 55–115, 1989.

[10] D. W. Schubert, J. S. Pepi, and F. E. Roman, "Investigation of the vibration isolation of commercial jet transport pilots during turbulent air penetration," NASA, Washington, DC, USA, Tech. Rep. NASA CR-1560, Jul. 1970.

[11] F. P. Dimasi, R. E. Allen, and P. C. Calcaterra, "Effect of vertical active vibration isolation on tracking performance and on ride qualities," NASA, Washington, DC, USA, Tech. Rep. NASA CR-2146, Nov. 1972.

[12] M. Velger, A. J. Grunwald, and S. J. Merhav, "Suppression of biodynamic disturbances and pilot-induced oscillations by adaptive filtering," *J. Guid. Control Dyn.*, vol. 7, no. 4, pp. 401–409, 1984.

[13] M. Velger, A. J. Grunwald, and S. J. Merhav, "Adaptive filtering of biodynamic stick feedthrough in manipulation tasks on board moving platforms," *J. Guid. Control Dyn.*, vol. 11, no. 2, pp. 153–159, 1988.

[14] D. W. Repperger, "Biodynamic and spasticity reduction in joystick control via force reflection," Armstrong Lab., Air Force Materiel Command, Wright-Patterson AFB, OH, USA, Tech. Rep. AL/CF-TR-1995-0152, Sep. 1995.

[15] S. Sövényi, "Model-based cancellation of biodynamic feedthrough with a motorized manual control interface," Ph.D. dissertation, Mech. Eng., Univ. Michigan, Ann Arbor, MI, USA, 2005.

[16] M. R. Sirouspour and S. E. Salcudean, "Suppressing operator-induced oscillations in manual control systems with movable bases," *IEEE Trans. Control Syst. Technol.*, vol. 11, no. 4, pp. 448–459, Jul. 2003.

[17] J. Venrooij, M. Mulder, M. M. van Paassen, D. A. Abbink, and M. Mulder, "A review of biodynamic feedthrough mitigation techniques," in *Proc. 11th IFAC/IFIP/IFORS/IEA Symp. Anal. Design Eval. Human Mach. Syst.*, vol. 11. Valenciennes, France, Sep. 2010, pp. 316–321.

[18] D. A. Abbink and M. Mulder, "Neuromuscular analysis as a guideline in designing shared control," in *Advances in Haptics*, M. H. Zadeh, Ed. Vukovar, Croatia: INTECH, Apr. 2010, ch. 27, pp. 499–516.

[19] J. Venrooij, D. A. Abbink, M. Mulder, M. M. van Paassen, and M. Mulder, "Biodynamic feedthrough is task dependent," in *Proc. IEEE Int. Conf. Syst. Man Cybern.*, Istanbul, Turkey, Oct. 2010, pp. 2571–2578.

[20] J. Venrooij, D. A. Abbink, M. Mulder, M. M. van Paassen, and M. Mulder, "A method to measure the relationship between biodynamic feedthrough and neuromuscular admittance," *IEEE Trans. Syst., Man, Cybern. B, Cybern.*, vol. 41, no. 4, pp. 1158–1169, Aug. 2011.

[21] J. Venrooij *et al.*, "Cancelling biodynamic feedthrough requires a subject and task dependent approach," in *Proc. IEEE Int. Conf. Syst. Man Cybern.*, Anchorage, AK, USA, Oct. 2011, pp. 1670–1675.

[22] D. A. Abbink, M. Mulder, F. C. T. van der Helm, M. Mulder, and E. R. Boer, "Measuring neuromuscular control dynamics during car following with continuous haptic feedback," *IEEE Trans. Syst., Man, Cybern. B, Cybern.*, vol. 41, no. 5, pp. 1239–1249, Oct. 2011.

[23] J. Venrooij *et al.*, "Mathematical biodynamic feedthrough model applied to rotorcraft," *IEEE Trans. Cybern.*, vol. 44, no. 7, pp. 1025–1038, Jul. 2014.

[24] D. T. McRuer and H. R. Jex, "A review of quasi-linear pilot models," *IEEE Trans. Human Factors Electron.*, vol. HFE-8, no. 3, pp. 231–249, Sep. 1967.

[25] J. Venrooij *et al.*, "A new view on biodynamic feedthrough analysis: Unifying the effects on forces and positions," *IEEE Trans. Cybern.*, vol. 43, no. 1, pp. 129–142, Feb. 2013.
[26] G. Torle, "Tracking performance under random acceleration: Effects of control dynamics," *Ergonomics*, vol. 8, no. 4, pp. 481–486, 1965.
[27] J. Venrooij *et al.*, "How effective is an armrest in mitigating biodynamic feedthrough?" in *Proc. IEEE Int. Conf. Syst. Man Cybern.*, Seoul, South Korea, Oct. 2012, pp. 2150–2155.
[28] R. W. Allen, H. R. Jex, and R. E. Magdaleno, "Manual control performance and dynamic response during sinusoidal vibration," Syst. Technol. Inc., Aerospace Med. Res. Lab., Hawthorne, CA, USA, Tech. Rep. AD-773844, Oct. 1973.
[29] M. Mulder and J. A. Mulder, "Cybernetic analysis of perspective flight-path display dimensions," *J. Guid. Control Dyn.*, vol. 28, no. 3, pp. 398–411, 2005.
[30] D. A. Abbink, "Neuromuscular analysis of haptic gas pedal feedback during car following," Ph.D. dissertation, Dept. Mech. Maritime Mater. Eng., Technische Universiteit Delft, Delft, The Netherlands, 2006.
[31] M. Olivari, F. M. Nieuwenhuizen, H. H. Bülthoff, and L. Pollini, "Identifying time-varying neuromuscular response: Experimental evaluation of a RLS-based algorithm," in *Proc. AIAA Model. Simulat. Technol. Conf.*, Kissimmee, FL, USA, Jan. 2015, pp. 1–15.
[32] J. Venrooij, M. Olivari, and H. H. Bülthoff, "Biodynamic feedthrough: Current status and open issues," in *Proc. 13th IFAC/IFIP/IFORS/IEA Symp. Anal. Design Eval. Human Mach. Syst.*, Kyoto, Japan, Sep. 2016, pp. 1–6.
[33] O. Stroosma, M. M. van Paassen, and M. Mulder, "Using the SIMONA research simulator for human-machine interaction research," in *Proc. AIAA Model. Simulat. Technol. Conf.*, Austin, TX, USA, Aug. 2003, pp. 1–8.
[34] S. Maddan, J. T. Walker, and J. M. Miller, "Does size really matter?: A reexamination of Sheldon's somatotypes and criminal behavior," *Soc. Sci. J.*, vol. 45, no. 2, pp. 330–344, 2008.
[35] R. Pintelon, P. Guillaume, Y. Rolain, J. Schoukens, and H. Van Hamme, "Parametric identification of transfer functions in the frequency domain: A survey," *IEEE Trans. Autom. Control*, vol. 39, no. 11, pp. 2245–2260, Nov. 1994.
[36] J. Venrooij *et al.*, "Admittance-adaptive model-based cancellation of biodynamic feedthrough," in *Proc. IEEE Int. Conf. Syst. Man Cybern.*, San Diego, CA, USA, Oct. 2014, pp. 1946–1951.

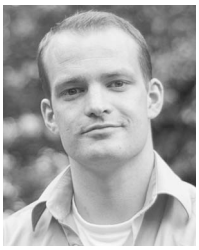

Joost Venrooij (S'10–M'14) received the M.Sc. and Ph.D. degrees (*cum laude*) in aerospace engineering from the Delft University of Technology, Delft, The Netherlands, in 2009 and 2014, respectively, with a focus on biodynamic feedthrough.

He is currently a Project Leader with the Max Planck Institute for Biological Cybernetics, Tübingen, Germany. His current research interests include biodynamic feedthrough, haptics support systems, and motion simulation.

Max Mulder received the M.Sc. and Ph.D. degrees (*cum laude*) in aerospace engineering from the Delft University of Technology, Delft, The Netherlands, in 1992 and 1999, respectively, with a focus on the cybernetics of tunnel-in-the-sky displays.

He is currently a Full Professor and the Head of the Control and Simulation Division, Faculty of Aerospace Engineering, Delft University of Technology. His current research interests include cybernetics and its use in modeling human perception and performance, and cognitive systems engineering and its application in the design of "ecological" human–machine interfaces.

Mark Mulder (M'08) received the M.Sc. degree in aerospace engineering from Vrije Universiteit Amsterdam, Amsterdam, The Netherlands, the Ph.D. degree in haptic driver support systems from the Delft University of Technology, Delft, The Netherlands, in 2000 and 2007, respectively, and the medical degree from the VUmc School of Medical Sciences, Amsterdam, in 2014.

He was a Post-Doctoral Research Fellow with the Biomechanical and Aerospace Engineering Departments, Delft University of Technology, where he is currently a Medical Doctor of Internal Medicine.

David A. Abbink (M'12–SM'14) received the M.Sc. and Ph.D. degrees in mechanical engineering from the Delft University of Technology, Delft, The Netherlands, in 2002 and 2006, respectively.

He is currently an Associate Professor with the Delft Haptics Laboratory, Delft University of Technology. His current research interests include neuromuscular behavior, driver support systems, and haptics.

Dr. Abbink is an Associate Editor of the IEEE TRANSACTIONS ON HUMAN–MACHINE SYSTEMS.

Marinus M. van Paassen (M'08–SM'15) received the M.Sc. and Ph.D. degrees from the Delft University of Technology, Delft, The Netherlands, in 1988 and 1994, respectively, with a focus on the role of the neuromuscular system of the pilot's arm in manual control.

He is an Associate Professor of Aerospace Engineering with the Delft University of Technology, researching on human–machine interaction and aircraft simulation. His current research interests include human–machine interaction that ranges from human manual control to complex cognitive systems.

Dr. van Paassen is an Associate Editor of the IEEE TRANSACTIONS ON HUMAN–MACHINE SYSTEMS.

Frans C. T. van der Helm received the M.Sc. degree in human movement science and the Ph.D. degree (*cum laude*) in mechanical engineering in 1985 and 1991, respectively.

He is a Professor of Biomechatronics and Bio-Robotics with the Delft University of Technology, Delft, The Netherlands, and an Adjunct Professor with the University of Twente, Enschede, The Netherlands, and Northwestern University, Evanston, IL, USA. He is one of the programme leaders in the Medical Delta, the NeuroSIPE Program, and H-Haptics Program. His current research interests include biomechanics of the upper and lower extremity, neuromuscular control, eye biomechanics, pelvic floor biomechanics, human motion control, and posture stability.

Prof. van der Helm was a recipient of an ERC Advanced Grant on "4D EEG: A new tool to assess the spatial and temporal activity in the cortex."

Heinrich H. Bülthoff (M'95) received the Ph.D. degree in natural sciences from Eberhard Karls University, Tübingen, Germany, in 1980.

He was a Research Scientist with the Max Planck Institute for Biological Cybernetics (MPI-KYB), Tübingen, from 1980 to 1985, and a Visiting Scientist with the Massachusetts Institute of Technology, Cambridge, MA, USA, from 1985 to 1988. From 1988 to 1993, he was an Assistant Professor, an Associate Professor, and finally a Full Professor of Cognitive Science with Brown University, Providence, RI, USA. In 1993, he became the Director of the Department of Human Perception, Cognition, and Action, MPI-KYB, and a Scientific Member of the Max Planck Society. Since 1996, he has been an Honorary Professor with Eberhard Karls University, and an Adjunct Professor with Korea University, Seoul, South Korea. His current research interests include object recognition and categorization, perception and action in virtual environments, and human–robot interaction.